Monika Koerber (Autor)

The rotational spectrum of oxatrisulfane and dimethyl ether 13C-isotopologues

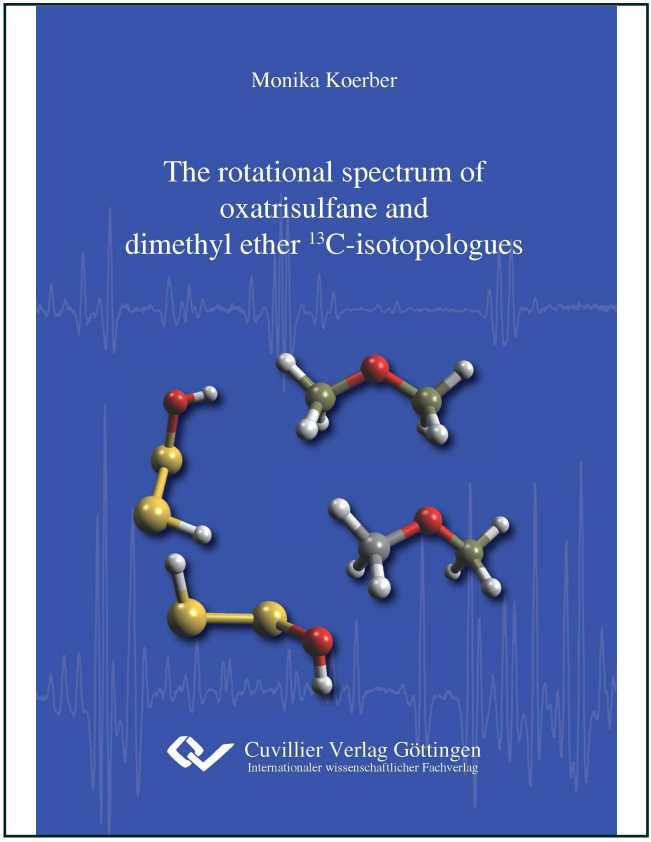

https://cuvillier.de/de/shop/publications/6421

1

Introduction

Both sulfur and oxygen belong to the sixth main group of the periodic table. Considering only the valence electronic configuration, they are expected to show similar characteristics in their chemical bondings. However, already in its elemental form sulfur occurs in many different configurations, whereas oxygen under standard conditions only forms the O_2 dimer. Polysulfanes H_2S_n and hydrogen oxides H_2O_n can appear in a large number of different configurations, as well. Their study enables to examine the electronic effects dominating the chemical bond which are responsible for the preference of certain molecular geometries over other possible configurations. Oxasulfanes, containing both sulfur and oxygen atoms, are a class of molecules where this investigation of the bonding mechanisms can be refined. Understanding the detailed characteristics of chemical bonds is crucial for the prediction of molecular conformation.
Most oxasulfanes are too unstable to be isolated in pure form. Consequently, the physical and chemical properties of these species are not well-known. Only in the last decade many experimental[1] and theoretical[2] studies have been performed on the smallest member of the familiy of oxasulfanes, 1-oxadisulfane (HSOH). In fact, a thorough gas-phase characterization using rotational spectroscopy and including determination of the molecular structure has so far only been accomplished for HSOH. Its empirical equilibrium structure, determined by Baum *et al.* in 2006 [4], proves HSOH to be the intermediate between the structures of its brethren molecules H_2S_2 and H_2O_2. All three molecules have the form of a twisted chain and exist in two energetically equal, chiral geometric structures. The molecule can convert into its chiral mirror image by internal rotation of one part of the molecule against the other.
For the next larger hydrogen compounds of oxygen and sulfur, the helical *trans*-form and the crown-like *cis*-form (see structures 1 and 1a in Fig. 1.1) are expected to be the most stable ones [61]. In case of H_2O_3 only the *trans* conformer has been observed and its structure has been determined by Suma *et al.*, but despite careful experimental effort no evidence of the *cis* structure has been found [95]. This indicates the *trans*-form to be the most stable conformation of this molecule. For H_2S_3 both structures, the *trans*- as well as the *cis*-form, have been observed by Liedtke *et al.* and the geometrical

[1] experimental studies by Winnewisser *et al.* (2003) [107], Behnke *et al.* (2003) [10], Brünken *et al.* (2005) [19], Beckers *et al.* (2006) [8], and Baum *et al.* (2006, 2008) [4, 5, 6]

[2] theoretical studies by Winnewisser *et al.* (2003) [107], Quack *et al.* (2003) [82], Yamada *et al.* (2004) [110], Denis *et al.* (2008) [29], and Ovsyannikov *et al.* (2008) [77]

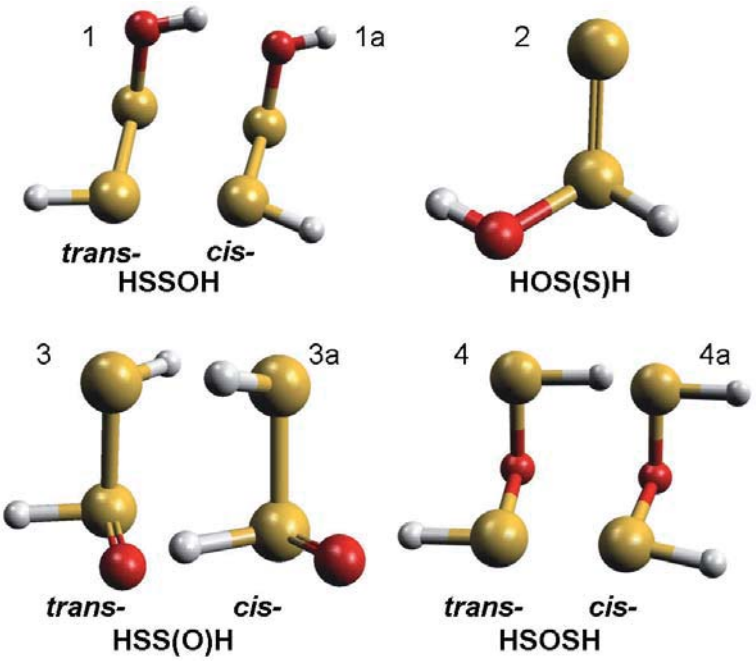

Figure 1.1: Isomeric structures of H_2S_2O with lowest energy according to Steudel *et al.* [94]

parameters have been derived from the obtained spectroscopic parameters [62]. The *trans* conformer was found to be slightly more stable by about 1 kJ/mol. Turning to the mixed species only very little is known so far. For a long time, the compound H_2S_2O was thought to have a branched structure with a S–O double bond and only the sulfur atoms in line [50] (see structure 3 in Fig. 1.1), but quantum-chemical calculations by Steudel *et al.* [94] revealed non-branched chain structures with *trans*- and *cis*-form to be more stable by more than 90 kJ/mol. *trans*-HSSOH was found to be energetically more stable than its *cis* conformer by about 4 kJ/mol. This result has been confirmed by high-level coupled-cluster calculations performed by Gauss *et al.* [36] (predicted energy difference of 2.0 kJ/mol) as well as by a study of Mikolajczyk *et al.* [69] (predicted energy difference smaller than 6 kJ/mol). Figure 1.1 shows a sketch of the four possible isomeric structures of H_2S_2O with lowest energy according to Steudel *et al.* [94]. First evidence for the formation of 1-oxatrisulfane, HSSOH, in the gas phase was found by Königshofen *et al.* monitoring the infrared bands of pyrolysis products of *tert*-butylthiosulfinic acid S-*tert*-butylester [57]. However, a conclusive proof for the formation of HSSOH and the unambiguous identification of different conformers is only possible by means of high-resolution rotational spectroscopy.

2

Theoretical considerations

Analyzing the spectra of rotating molecules requires knowledge of their rotational energies, allowed transitions and their intensities. The fundamental theoretical aspects concerning these topics are briefly summarized in the following sections. They are based mainly on the textbooks by Gordy & Cook [39] and Bernath [15].

2.1 Rotational energy

The classical expression for the rotational kinetic energy of a rigid body is given by

$$E_{\mathrm{rot}} = \frac{1}{2}\vec{\omega}^{t}\mathbf{I}\vec{\omega} \tag{2.1}$$

$$= \frac{1}{2}I_{xx}\omega_x^2 + \frac{1}{2}I_{yy}\omega_y^2 + \frac{1}{2}I_{zz}\omega_z^2 + I_{xy}\omega_x\omega_y + I_{xz}\omega_x\omega_z + I_{yz}\omega_y\omega_z \tag{2.2}$$

where $\vec{\omega}$ is the angular velocity and $\mathbf{I}$ is the moment of intertia tensor. x, y, z are the positional coordinates of the rotating body relative to a rectangular coordinate system fixed in the body with its origin at the center of mass.
With $\vec{e_x}$, $\vec{e_y}$, $\vec{e_z}$ unit vectors of the body-fixed system, the moment of inertia tensor is defined as

$$\begin{aligned}\mathbf{I} = {} & I_{xx}\vec{e_x}\vec{e_x} + I_{xy}\vec{e_x}\vec{e_y} + I_{xz}\vec{e_x}\vec{e_z} \\ & + I_{yx}\vec{e_y}\vec{e_x} + I_{yy}\vec{e_y}\vec{e_y} + I_{yz}\vec{e_y}\vec{e_z} \\ & + I_{zx}\vec{e_z}\vec{e_x} + I_{zy}\vec{e_z}\vec{e_y} + I_{zz}\vec{e_z}\vec{e_z}\end{aligned} \tag{2.3}$$

with

$$\begin{aligned} I_{xx} &= \sum_i m_i(y^2+z^2) \\ I_{yy} &= \sum_i m_i(x^2+z^2) \\ I_{zz} &= \sum_i m_i(x^2+y^2) \\ I_{xy} &= I_{yx} = -\sum_i m_i xy \\ I_{zx} &= I_{xz} = -\sum_i m_i xz \\ I_{yz} &= I_{zy} = -\sum_i m_i yz \end{aligned} \tag{2.4}$$

where m_i is the mass of a particular particle of the body.
According to classical mechanics it is always possible to choose the coordinate system in such a way that the non-diagonal elements of the moments of inertia tensor vanish, leaving only the so-called principal moments of inertia on the diagonal. If a, b, and c denote the principal axes, equation (2.2) becomes

$$\begin{aligned} E_{\text{rot}} &= \frac{1}{2}I_a\omega_a^2 + \frac{1}{2}I_b\omega_b^2 + \frac{1}{2}I_c\omega_c^2 \\ &= \frac{J_a^2}{2I_a} + \frac{J_b^2}{2I_b} + \frac{J_c^2}{2I_c} \end{aligned} \tag{2.5}$$

where $J_{a,b,c}$ denote the components of the total angular momentum vector $\vec{J}$.

There are six different ways to map (x,y,z) into (a,b,c) (see Table 2.1). Though the choice of the identification is arbitrary, the x,y,z axes are usually picked according to a set of common conventions in spectroscopy: The z-axis of a molecule is always chosen to be the highest order axis of rotatioal symmetry, and the x-axis is out of plane for a planar molecule. The identification to (a,b,c) is chosen in such a way that $I_a \le I_b \le I_c$ becomes true, i.e. that I_c is always the largest moment of inertia and I_a is the smallest.

Table 2.1: Identification of the (x,y,z) axis system with the a,b,c axes. The superscripts r and l denote the right- and left-handed orientation of the (a,b,c) axis system.

	I^r	II^r	III^r	I^l	II^l	III^l
x	b	c	a	c	a	b
y	c	a	b	b	c	a
z	a	b	c	a	b	c

Molecules are classified according to the values of their principal moments of inertia. There are five cases:

- Linear molecules: $I_a = 0$, $I_b = I_c$
- Spherical symmetric tops: $I_a = I_b = I_c$
- Prolate symmetric tops: $I_a < I_b = I_c$
- Oblate symmetric tops: $I_a = I_b < I_c$
- Asymmetric tops: $I_a < I_b < I_c$

All molecules studied in the scope of this thesis are asymmetric rotors close to the limiting case of a prolate symmetric top. Therefore, the theoretical details considering symmetric and asymmetric tops are briefly discussed in the following.

2.2 Symmetric top molecules

In a symmetric top, one of the principal axes of inertia must lie along the molecular axis of symmetry. The other principal moments of inertia, which have their axes perpendicular to the symmetry axis, are equal. In a prolate symmetric top, the molecular axis of symmetry is the a-axis, i.e. the axis of the smallest moment of inertia ($I_a < I_b = I_c$). In an oblate symmetric top, the symmetry axis is the c-axis with the largest moment of inertia ($I_a = I_b < I_c$).
In the following, the treatment of symmetric tops will be limited to the case of a prolate top. The results also apply to oblate tops by interchanging the labels a and c.

2.2.1 Rigid symmetric rotor

The corresponding quantum mechanical Hamiltonian to equation (2.5) is

$$\hat{H}_r = \frac{\hat{J}_a^2}{2I_a} + \frac{\hat{J}_b^2}{2I_b} + \frac{\hat{J}_c^2}{2I_c} \tag{2.6}$$

with $\hat{\boldsymbol{J}}^2 = \hat{J}_a^2 + \hat{J}_b^2 + \hat{J}_c^2$ for the operator of total angular momentum. Due to $I_b = I_c$ for a prolate rotor one obtains

$$\hat{H}_r = \frac{1}{2I_b}\hat{\boldsymbol{J}}^2 + \left(\frac{1}{2I_a} - \frac{1}{2I_b}\right)\hat{J}_a^2 \tag{2.7}$$

The angular momentum operators $\hat{\boldsymbol{J}}^2$, $\hat{J}_z$ (Projection onto the z-axis of the molecule-fixed (x,y,z) coordinate system), and $\hat{J}_Z$ (Projection onto the Z-axis of the space-fixed (X,Y,Z) cartesian coordinates) all commute with the Hamiltonian $\hat{H}_r$, so that a set of simultaneous eigenfunctions $|J,K,M\rangle$ can be found (see e.g. [39]), with eigenvalues

$$\begin{aligned} \langle J,K,M|\hat{\boldsymbol{J}}^2|J,K,M\rangle &= \hbar^2 J(J+1) \\ \langle J,K,M|\hat{J}_z|J,K,M\rangle &= \hbar K \\ \langle J,K,M|\hat{J}_Z|J,K,M\rangle &= \hbar M \end{aligned} \tag{2.8}$$

and the quantum numbers

$$\begin{aligned} J &= 0,1,2,3,... \\ K &= 0,\pm1,\pm2,\pm3,...,\pm J \\ M &= 0,\pm1,\pm2,\pm3,...,\pm J \end{aligned}$$

The symmetric top eigenfunctions $|J,K,M\rangle$ have the form (see [111])

$$|J,K,M\rangle = \left[\frac{2J+1}{8\pi^2}\right]^{1/2} e^{iM\phi} d^{(J)}_{MK}(\theta) e^{iK\chi} \tag{2.9}$$

where ϕ, θ, and χ are the Euler-angles describing the orientation of the molecule-fixed coordinate system with respect to the space-fixed laboratory system, and the $d^{(J))}_{MK}$ are hypergeometric functions of $\sin^2(\theta/2)$.

The eigenvalues of the symmetric top Hamiltonian (eq. (2.7)) are the quantized rotational energies, obtained by solving the Schrödinger equation

$$\hat{H}_r|J,K,M\rangle = E|J,K,M\rangle \tag{2.10}$$

using the eigenvalues of the angular momentum operators[1] given in equation (2.9). It follows

$$\begin{aligned} E_{\text{prolate}}(J,K_a) &= \frac{\hbar^2}{2I_b}J(J+1) + \left(\frac{\hbar^2}{2I_a} - \frac{\hbar^2}{2I_b}\right)K_a^2 \\ &= BJ(J+1) + (A-B)K_a^2 \end{aligned} \tag{2.11}$$

$$\begin{aligned} E_{\text{oblate}}(J,K_c) &= \frac{\hbar^2}{2I_b}J(J+1) + \left(\frac{\hbar^2}{2I_c} - \frac{\hbar^2}{2I_b}\right)K_c^2 \\ &= BJ(J+1) + (C-B)K_c^2 \end{aligned} \tag{2.12}$$

with the rotational constants in energy units

$$\begin{aligned} A &= \frac{\hbar^2}{2I_a} \\ B &= \frac{\hbar^2}{2I_b} \\ C &= \frac{\hbar^2}{2I_c} \end{aligned} \tag{2.13}$$

All energy levels except for $K=0$ are doubly degenerated since K appears as a squared term in equations (2.11) and (2.12). In addition to the K degeneracy, there is a $(2J+1)$ degeneracy for the field-free rotor due to the M quantum number. This degeneracy can be completely lifted by applying an external electrical or magnetical field, which would have to be treated as an additional term in the Hamiltonian.

[1] The subscripts a and c are used with the quantum number K in order to specify the z-axis of projection, which is the a-axis in case of a prolate symmetric top and the c-axis for an oblate top.

2.2.2 Centrifugal distortion

In the previous section, the molecule was considered as rigid. However, as a molecule rotates, its bond distances and angles vary due to centrifugal forces which equilibrate with the restoring potential forces. The centrifugal stretching of the molecule is treated as a pertubation on the eigenstates of the rigid rotor. If $\hat{H}_r$ is the Hamiltonian of the rigid rotor and $\hat{H}_d$ represents that of the distortional energy, the total Hamiltonian is

$$\hat{H} = \hat{H}_r + \hat{H}_d \tag{2.14}$$

In [39] it is shown that the centrifugal distortional Hamiltonian has the form

$$\hat{H} = \frac{\hbar^4}{4} \sum_{\alpha,\beta,\gamma,\delta} \tau_{\alpha,\beta,\gamma,\delta} \hat{J}_\alpha \hat{J}_\beta \hat{J}_\gamma \hat{J}_\delta \tag{2.15}$$

with the centrifugal distortion constants

$$\tau_{\alpha,\beta,\gamma,\delta} = -\frac{1}{2} \sum_{ij} \mu^{(i)}_{\alpha\beta} (f^{-1})_{ij} \mu^{(j)}_{\gamma\delta} \tag{2.16}$$

The coefficient $\mu^{(i)}_{\alpha\beta}$ is the partial derivative of the $\alpha\beta$ component of the inverse moment of inertia tensor with respect to the internal coordinate i.
$(f^{-1})_{ij}$ is an element of the reciprocal matrix of the force constants f_{ij}. Each of the operators $\hat{J}_\alpha$, $\hat{J}_\beta$, $\hat{J}_\gamma$, and $\hat{J}_\delta$ represents an angular momentum about one of the principal coordinate axes of the molecule (they are not all different, and all may even be the same).
In first-order pertubation treatment (shown in detail in [39]) the distortional Hamiltonian (2.15) can be simplified for a symmetric top giving rise to the first-order distortional energy

$$E^{(1)}_d = -[D_J J^2 (J+1)^2 + D_{JK} J(J+1) K^2 + D_K K^4] \tag{2.17}$$

D_J, D_{JK}, and D_K are the first-order centrifugal distortion contants of the symmetric top molecule.

2.2.3 Selection rules

Transitions between the energy states of a symmetric rotor are induced, if electromagnetic radiation interacts with a permanent electric or magnetic dipole moment component of the molecule. Since the electric and magnetic fields are fixed in space, but the dipole moment of the molecule is fixed to the rotating body, the direction cosine matrix elements of the molecule-fixed axes relative to the space-fixed axes of the laboratory frame have to be considered to derive the selection rules for rotational transitions, transition probabilities, and intensities. A detailed derivation can be found for example in the textbook by Gordy & Cook [39]. Transitions are allowed, if not all components of the transition dipole moment matrix

$$\mathbf{M} = \int \langle J'K'M' | \hat{\mu}_F | J''K''M'' \rangle \, d\tau \quad \text{with} \quad F = X, Y, Z \tag{2.18}$$

vanish. In a symmetric top, the permanent dipole moment $\vec{\mu}$ must lie along the symmetry axis. All matrix elements of the transition dipole moment $\mathbf{M}$ along a space-fixed axis vanish except those between states with $J'' = J'$ or $J'' = J' \pm 1$, $K'' = K'$, and $M'' = M'$ or $M'' = M' \pm 1$. The selection rules for a symmetric rotor are therefore

$$\Delta J = 0, \pm 1, \quad \Delta K = 0, \quad \Delta M = 0, \pm 1 \tag{2.19}$$

Application of these rules to the energy terms of a symmetric top (eq. (2.11) with centrifugal distortional energy (2.17)) gives rise to the formula for the absorption frequencies

$$\nu_{J+1,K \leftarrow J,K} = 2B(J+1) - 4D_J(J+1)^3 - 2D_{JK}(J+1)K^2 \tag{2.20}$$

Due to $\Delta K = 0$ the transitions are confined to lie within a K-stack for a given $J+1 \leftarrow J$. The effect of the centrifugal distortion constant D_{JK} splits up transitions with different values of $|K|$.

2.3 Asymmetric top molecules

For an asymmetric top molecule, all principal moments of inertia are different and none of them is zero ($I_a < I_b < I_c$). The total angular momentum has projections on all principal axes and no component is a constant of the motion, i.e. $\hat{J}_z$ no longer is a "good" quantum number. Only the total angular momentum $\hat{J}$ and the projection on the space-fixed Z-axis are conserved with rotation of the molecule and commute with the Hamiltonian $\hat{H}$. In contrast to the symmetric top, the rotational frequencies can no longer be expressed in convenient equations, even if centrifugal distortion effects are neglected.
As a measure of the asymmetry of a molecule the parameter κ is used, the so-called *Ray's asymmetry parameter*:

$$\kappa = \frac{2B - A - C}{A - C} \tag{2.21}$$

The limiting cases of κ, -1 and $+1$, correspond to the prolate and the oblate symmetric top, respectively. They are the simple limiting cases of the asymmetric rotor. Therefore, the projections of the total angular momentum on the a- and the c-axis of the molecule-fixed principal axes system are used as "pseudo" quantum numbers to label the energies of the asymmetric rotor. In this thesis, the double-subscript system introduced by King *et al.* [54] is used, which is best understood by correlating the energies of the limiting cases of prolate and oblate symmetric top (see Fig. 2.1). The energies of the asymmetric rotor differ from the symmetric top in that the levels corresponding to $-K$ and $+K$, which are always degenerate for the symmetric top, are separated for the asymmetric rotor. For each value of J, the asymmetric rotor has $(2J+1)$ distinct rotational sublevels. With an increase of asymmetry, the "K-splitting" becomes larger, and there is no longer a close correspondence of these two levels to the degenerate K levels of the symmetric top. K_a and K_c are far from being "good" quantum numbers and the double-subscript is just used as a label.

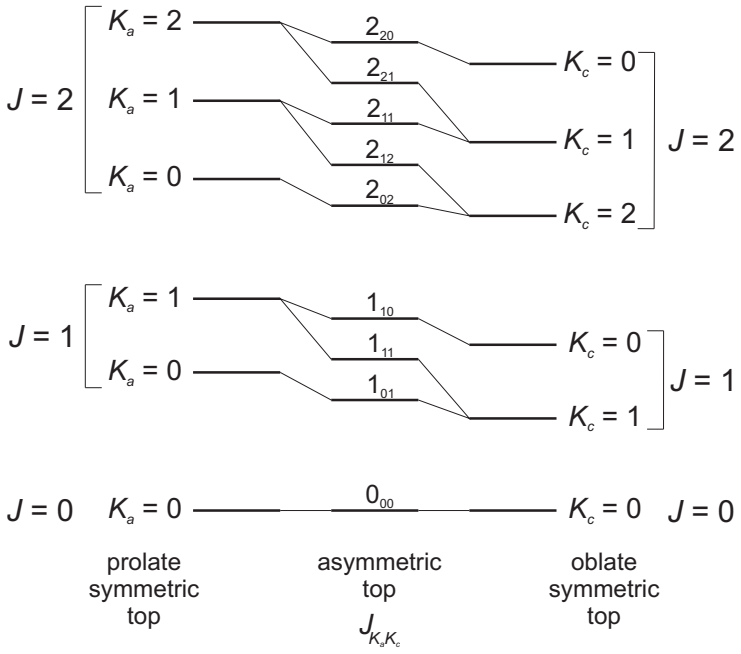

Figure 2.1: Prolate-oblate correlation diagram used to label the asymmetric rotor energy levels[2]. The energy levels are not to scale and the lines connecting the prolate to the oblate levels correspond to a hypothetical distortion of a molecule from a prolate to an oblate top.

2.3.1 Rigid asymmetric rotor

The Hamiltonian for a rigid asymmetric rotor is given by

$$\hat{H} = \frac{\hat{J}_a^2}{2I_a} + \frac{\hat{J}_b^2}{2I_b} + \frac{\hat{J}_c^2}{2I_c} \tag{2.22}$$

As mentioned above, the projection onto none of the principal axes is a constant to the motion. Therefore, unlike for the symmetric top, the Schrödinger equation cannot be solved directly. Only for certain low J values the energies can be expressed in closed form. The general procedure is to represent the asymmetric rotor wave functions $|J, K_a K_c, M\rangle$ by a linear combination of symmetric top wave functions:

$$|J, K_a K_c, M\rangle = \sum_{J,K,M} a_{JKM} |J, K, M\rangle \tag{2.23}$$

where a_{JKM} are numerical constants.
For convenience, the Hamiltonian in eq. (2.22) is rewritten using the lowering and raising operators (in I^r representation) $\hat{J}_+ = \hat{J}_b + i\hat{J}_c$ and $\hat{J}_- = \hat{J}_b - i\hat{J}_c$ with

$$\begin{aligned}
\langle J, K-2, M| \hat{J}_+^2 |J, K, M\rangle &= \hbar^2 \sqrt{(J+K)(J-K+1)(J+K-1)(J-K+2)} \\
\langle J, K+2, M| \hat{J}_-^2 |J, K, M\rangle &= \hbar^2 \sqrt{(J-K)(J+K+1)(J-K-1)(J+K+2)}
\end{aligned} \tag{2.24}$$

[2]Reproduced after Figure 6.33 of [15]

Using the definitions for the rotational constants given in eq. (2.14), the Hamiltonian (2.22) becomes

$$\begin{aligned}\hbar\hat{H} &= A\hat{J}_a^2 + B\hat{J}_b^2 + C\hat{J}_c^2 \\ &= \left(\frac{B+C}{2}\right)(\hat{J}_b^2 + \hat{J}_c^2) + A\hat{J}_a^2 + \left(\frac{B-C}{2}\right)(\hat{J}_b^2 - \hat{J}_c^2) \\ &= \left(\frac{B+C}{2}\right)\hat{\boldsymbol{J}}^2 + \left(A - \frac{B+C}{2}\right)\hat{J}_a^2 + \left(\frac{B-C}{4}\right)(\hat{J}_+^2 - \hat{J}_-^2)\end{aligned} \tag{2.25}$$

The eigenvalues of this Hamiltonian (and the numerical constants of eq. (2.23)) are determined by solving the secular determinant, which can be broken down into sub-determinants corresponding to each value of J.

2.3.2 Centrifugal distortion

Like for symmetric rotors, the Hamiltonian for the distorted asymmetric rotor is given by

$$\hat{H} = \hat{H}_r + \hat{H}_d \tag{2.26}$$

The centrifugal distortional Hamiltonian $\hat{H}_d$ (eq. (2.15)) depends on the constants $\tau_{\alpha,\beta,\gamma,\delta}$ and the angular momentum operators. A simple closed-form expression for the effect of these operators, like the one obtained for the symmetric rotor, cannot be obtained for an asymmetric rotor. A first-order pertubation treatment has been introduced by Kivelson and Wilson [56]. Watson has shown, that a maximum of five linear combinations of the nine possible τ's, i.e. no more than five centrifugal distortion constants, can be obtained from the analysis of a spectrum of an asymmetric rotor [102]. To properly fit experimental data, a reduced Hamiltonian has to be employed, from which all experimentally indeterminable parameters have been removed. This is done by a series of contact transformations.

Rotational Hamiltonian in A-reduction

Watson introduced a reduced Hamiltonian for asymmetric rotors that includes centrifugal distortion effects up to the sixth order of the angular momentum [103].

$$\hat{H}^{(A)} = \hat{H}_r + \hat{H}_d^{(4)} + \hat{H}_d^{(6)} \tag{2.27}$$

with

$$\begin{aligned}\hat{H}_r &= B_x^{(A)}\hat{J}_x^2 + B_y^{(A)}\hat{J}_y^2 + B_z^{(A)}\hat{J}_z^2 \\ &= \left(\frac{B_x^{(A)} + B_y^{(A)}}{2}\right)\hat{\boldsymbol{J}}^2 + \left(B_z^{(A)} - \frac{B_x^{(A)} + B_y^{(A)}}{2}\right)\hat{J}_z^2 + \left(\frac{B_x^{(A)} - B_y^{(A)}}{2}\right)(\hat{J}_x^2 - \hat{J}_y^2)\end{aligned} \tag{2.28}$$

$$\begin{aligned}\hat{H}_d^{(4)} &= \Delta_J \hat{J}^4 - \Delta_{JK}\hat{\boldsymbol{J}}^2\hat{J}_z^2 - \Delta_K \hat{J}_z^4 \\ &\quad -2\delta_J\hat{\boldsymbol{J}}^2(\hat{J}_x^2 - \hat{J}_y^2) - \delta_K[\hat{J}_z^2(\hat{J}_x^2 - \hat{J}_y^2) + (\hat{J}_x^2 - \hat{J}_y^2)\hat{J}_z^2]\end{aligned} \tag{2.29}$$

$$\begin{aligned}\hat{H}_d^{(6)} &= \Phi_J \hat{J}^6 + \Phi_{JK}\hat{J}^4\hat{J}_z^2 + \Phi_{KJ}\hat{\boldsymbol{J}}^2\hat{J}_z^4 + \Phi_K\hat{J}_z^6 \\ &\quad +2\phi_J\hat{J}^4(\hat{J}_x^2 - \hat{J}_y^2) \\ &\quad +\phi_{JK}\hat{\boldsymbol{J}}^2[\hat{J}_z^2(\hat{J}_x^2 - \hat{J}_y^2) + (\hat{J}_x^2 - \hat{J}_y^2)\hat{J}_z^2] \\ &\quad +\phi_K[\hat{J}_z^4(\hat{J}_x^2 - \hat{J}_y^2) + (\hat{J}_x^2 - \hat{J}_y^2)\hat{J}_z^4]\end{aligned} \tag{2.30}$$

where

$B_x^{(A)}$, $B_y^{(A)}$, $B_z^{(A)}$: rotational constant[3]
Δ_J, Δ_{JK}, Δ_K, δ_J, δ_K : quartic centrifugal distortion constants
Φ_J, Φ_{JK}, Φ_{KJ}, Φ_K, ϕ_J, ϕ_{JK}, ϕ_K : sextic centrifugal distortion constants

Note that $\hat{J}_z^2$ and $(\hat{J}_x^2 - \hat{J}_y^2)$ do not commute. The correlation of the centrifugal distortion coefficients of the reduced Hamiltonian and the distortion coefficients τ are listed in [39].

Rotational Hamiltonian in S-reduction

For only slightly asymmetric tops the choice of the five centrifugal distortion coefficients of the A-reduction are not very well suited, as has been pointed out by Carpenter [22]. Since the selection of distortion constants can be made in numerous ways, Winnewisser [106] and Van Eijck [100] proposed an alternate reduction of the Hamiltonian that reduces in a well-defined way to the symmetric top limit. It was extended by Typke [99] to the sixth order in angular momentum, and he demonstrated that this Hamiltonian yields better convergence for molecules very close to the symmetric top limit.

$$\hat{H}^{(S)} = \hat{H}_r + \hat{H}_d^{(4)} + \hat{H}_d^{(6)} \tag{2.31}$$

[3] In I^r-representation $B_x^{(A)}$, $B_y^{(A)}$, and $B_z^{(A)}$ correspond to the rotational constants B, C, and A, respectively.

with

$$\begin{aligned}\hat{H}_r &= B_x^{(S)}\hat{J}_x^2 + B_y^{(S)}\hat{J}_y^2 + B_z^{(S)}\hat{J}_z^2 \\ &= \left(\frac{B_x^{(S)}+B_y^{(S)}}{2}\right)\hat{\boldsymbol{J}}^2 + \left(B_z^{(S)} - \frac{B_x^{(S)}+B_y^{(S)}}{2}\right)\hat{J}_z^2 + \left(\frac{B_x^{(S)}-B_y^{(S)}}{4}\right)(\hat{J}_+^2 + \hat{J}_-^2)\end{aligned} \tag{2.32}$$

$$\hat{H}_d^{(4)} = -D_J\hat{J}^4 - D_{JK}\hat{\boldsymbol{J}}^2\hat{J}_z^2 - D_K\hat{J}_z^4 + d_1\hat{\boldsymbol{J}}^2(\hat{J}_+^2 + \hat{J}_-^2) + d_2(\hat{J}_+^4 + \hat{J}_-^4) \tag{2.33}$$

$$\begin{aligned}\hat{H}_d^{(6)} &= H_J\hat{J}^6 + H_{JK}\hat{J}^4\hat{J}_z^2 + H_{KJ}\hat{\boldsymbol{J}}^2\hat{J}_z^4 + H_K\hat{J}_z^6 \\ &\quad + h_1\hat{J}^4(\hat{J}_+^2 + \hat{J}_-^2) + h_2\hat{\boldsymbol{J}}^2(\hat{J}_+^4 + \hat{J}_-^4) + h_3(\hat{J}_+^6 + \hat{J}_-^6)\end{aligned} \tag{2.34}$$

where

$B_x^{(S)}$, $B_y^{(S)}$, $B_z^{(S)}$: rotational constant[4]
D_J, D_{JK}, D_K, d_1, d_2 : quartic centrifugal distortion constants
H_J, H_{JK}, H_{KJ}, H_K, h_1, h_2, h_3 : sextic centrifugal distortion constants

The coefficients in $\hat{H}^{(A)}$ and $\hat{H}^{(S)}$ can be related to each other as given in Table 2.2, and the coefficients of the two reduced Hamiltonians provide the same information. Both Hamiltonians can easily be further extended to higher orders.

Table 2.2: Relations between the coefficients of the A and S reduced Hamiltonians.[5]

$B_x^{(A)} = B_x^{(S)} - 4(2\sigma+1)d_2$	$B_y^{(A)} = B_y^{(S)} + 4(2\sigma-1)d_2$	$B_z^{(A)} = B_z^{(S)} + 10d_2$
$\Delta_J = D_J - 2d_2$	$\Delta_{JK} = D_{JK} + 12d_2$	$\Delta_K = D_K - 10d_2$
$\delta_J = -d_1$	$\delta_K = -4\sigma d_2$	
$\Phi_J = H_J + 2h_2$		$\Phi_{JK} = H_{JK} - 12h_2 + 16\sigma h_3$
$\Phi_{KJ} = H_{KJ} + 10h_2 - (160\sigma/3)h_3$		$\Phi_K = H_K + (112\sigma/3)h_3$
$\phi_J = h_1 + h_3$		
$\phi_{JK} = 4\sigma h_2 - 10h_3 - 8d_2(D_{JK} + 2\sigma d_1 + 4d_2)/(B_x - B_y)$		
$\phi_K = (32\sigma^2/3 + 9)h_3 - 16d_2(D_K + 2(\sigma^2-2)d_2)/(B_x - B_y)$		

$\sigma = (2B_z - B_x - B_y)/(B_x - B_y)$ as defined by Watson [103]

2.3.3 Selection rules

In contrast to the symmetric rotor, an arbitrary asymmetric rotor can have three dipole moment components μ_a, μ_b, and μ_c along the principal axes. Each nonvanishing dipole moment component leads to a set of selection rules for the pseudo quantum numbers K_a, K_c and gives rise to a certain set of transitions, the so-called a-type, b-type, and c-type transitions, respectively. The individual selection rules for these types of transitions are given in Table 2.3. The general selection rules on J and M are the same as for the symmetric rotor: $\Delta J = 0, \pm 1$ and $\Delta M = 0, \pm 1$.

[4] In I^r-representation $B_x^{(S)}$, $B_y^{(S)}$, and $B_z^{(S)}$ correspond to the rotational constants B, C, and A, respectively.
[5] Reproduced after Table 8.16 of [39]

Table 2.3: Selection rules for asymmetric top molecules

transition	dipole moment component	ΔK_a	ΔK_c
a-type	$\mu_a \neq 0$	0, (±2, ±4, ...)	±1, (±3, ±5, ...)
b-type	$\mu_b \neq 0$	±1, (±3, ±5, ...)	±1, (±3, ±5, ...)
c-type	$\mu_c \neq 0$	±1, (±3, ±5, ...)	0, (±2, ±4, ...)

The transitions given in brackets are much weaker than the main ones.

Sets of transitions with the same selection rules are often referred to as branches. A common notation (see e.g. in the textbook by Bernath [15]) to label those branches is

$$^{\Delta K_a}\Delta J_{K_a''}$$

where $\Delta J = -1, 0, 1$ is indicated by the characters P, Q, R, respectively, and $\Delta K_a = -1, 0, 1$ is related to p, q, r, respectively. K_a'' is the quantum number of the projection of the total angular momentum onto the molecule-fixed a-principal axis. Since all molecules that have been investigated in this thesis are close to the limiting case of a prolate symmetric top, K_a is almost a "good" quantum number for these molecules and indicates the rate of rotation around the molecular symmetry axis.

2.4 Spectral line intensities

The absolute intensity I of a spectral absorption line is given by

$$I = \int_0^\infty \alpha_\nu \, d_\nu \tag{2.35}$$

where α_ν is the absorption coefficient.
The absorption coefficient determines the power loss of radiation travelling through an absorption cell of length x. When P_0 is the input power, the power at the output P_x is given by Beer's Law[6]

$$P_x = P_0 \exp(-\alpha_\nu x) \tag{2.36}$$

The absorption coefficient mainly depends on the number N of molecules per unit volume in the absorption cell, the fraction f of these molecules in the lower state of the transition, and on the size of the dipole moment matrix element μ_{ij} for the transition from the lower rotational state i to the higher state j, summed over the three perpendicular directions in space.

$$\alpha_\nu = \frac{8\pi^3 N f \nu^3}{3ckT}\left(1 - \frac{1}{2}\frac{h\nu}{kT}\right)|\mu_{ij}|^2 S(\nu, \nu_0) \tag{2.37}$$

with

$$|\mu_{ij}|^2 = |\langle j|\mu_X|i\rangle|^2 + |\langle j|\mu_Y|i\rangle|^2 + |\langle j|\mu_Z|i\rangle|^2 \tag{2.38}$$

where

$$\langle j|\mu_F|i\rangle = \int \psi_j^* \mu_F \psi_i \, d_\tau \quad \text{with} \quad F = X, Y, Z \tag{2.39}$$

[6] a detailed derivation of Beer's Law as well as the absorption coefficient can be found in textbooks e.g. by Gordy & Cook [39]

The parameter $S(\nu, \nu_0)$ in eq.(2.37) is the line-shape function. Due to various disturbances the energy levels are not completely sharp resulting in broadening of the spectral lines. Sources of line broadening are among others the natural line width, which arises from the limited lifetime of the molecule in the excited state, and the pressure broadening due to collisions between molecules, which terminates the lifetime of a molecule in a particular rotational state. These effects result in a Lorentzian shape of the absorption line. Another effect, the Doppler broadening, is the dominant line broadening effect in the measurements performed in the course of this thesis. The molecules of a gas at thermal equilibrium have a Maxwell-Boltzmann distribution of velocities. Due to the Doppler effect, the frequency of radiation absorbed depends on the velocity of the molecule relative to that of the radiation. The various Doppler shifts of all the molecular frequencies gives rise to a Gaussian line-shape function

$$S(\nu, \nu_0) = S_0 \ \exp\left[-\frac{mc^2}{2kT}\left(\frac{\nu - \nu_0}{\nu_0}\right)^2\right] \tag{2.40}$$

3

Synthesis of 1-oxatrisulfane

1-Oxatrisulfane is too reactive to be isolated in pure form. To study this molecule by means of gas phase spectroscopy, it has to be produced *in situ* during spectroscopic measurements to ensure a stable amount of sample in the absorption cell. Königshofen *et al.* [57] found first evidence for the formation of HSSOH in the gas phase by employing flash vacuum pyrolysis on the precursor molecule *tert*-butylthiosulfinic acid S-*tert*-butylester. The resulting pyrolysis products have been identified by their infrared absorption bands. M. Behnke recorded in his PhD thesis the relative amount of some pyrolysis products as a function of the pyrolysis temperature using a quadrupol mass spectrometer [9]. A more detailed study of the temperature dependence of pyrolysis products has been given in my diploma thesis [58]. In this work, a combination of infrared and rotational spectroscopy was employed to monitor the intensity of spectral features of pyrolysis products (either infrared absorption bands or rotational absorption lines) as a function of the pyrolysis temperature. In the course of this thesis, the synthesis conditions for HSSOH have been optimized, based on the results of the diploma thesis, which finally enabled its rotational spectroscopic detection given in Chapter 5.

3.1 Pyrolysis pathway

The synthesis of 1-oxatrisulfane by flash vacuum pyrolysis of *tert*-butylthiosulfinic acid S-*tert*-butylester, *t*-BuS(O)S*t*-Bu, proceeds in two steps (see Fig. 3.1). At temperatures between 300–500°C and pressures below 1 mbar, *tert*-butylthiosulfoxylic acid, *t*-BuSSOH, is formed by elimination of 2-methylpropene, C_4H_8. The intermediate pyrolysis product *t*-BuSSOH is proposed by Königshofen *et al.* to form its unbranched structure rather than occur as the branched isomer *t*-BuS(S)OH [57]. At higher temperatures, between 500–700°C, a second 2-methylpropene is eliminated and *t*-BuSSOH decomposes into 1-oxatrisulfane.

Figure 3.2 shows the temperature dependence of the intensities (relative to the corresponding maximum) as a function of the pyrolysis temperature for the precursor molecule *t*-BuS(O)S*t*-Bu (black data points), the intermediate *t*-BuSSOH (shown in red), and the byproduct of both pyrolysis steps 2-methylpropene (depicted in blue)

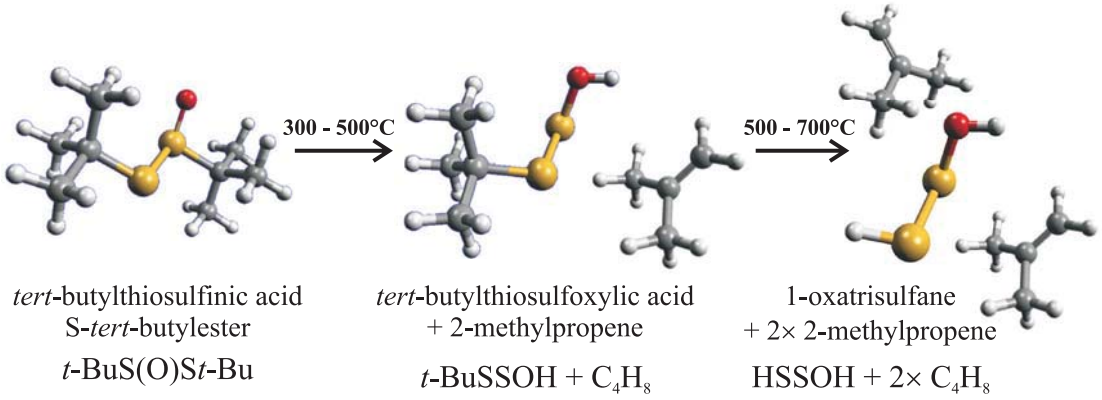

Figure 3.1: Synthesis of HSSOH by pyrolysis of *t*-BuS(O)S*t*-Bu. The reaction pathway is given according to Königshofen *et al.* [57]. The temperature spans for the different reaction steps are based on the studies performed in my diploma thesis [58] with the results summarized in Figure 3.2.

based on the results of my diploma thesis [58].[1] In case of 2-methylpropene, additional measurements of rotational lines were available, and their relative intensities have been averaged with the results from the infrared absorption measurements. The size of the error bars in Fig. 3.2 is given by the standard deviation from the mean value of line intensities measured during warm-up and cool-down of the pyrolysis oven. The trends in Figure 3.2 support the chemical synthesis pathway given by Königshofen *et al.* [57] shown in Fig. 3.1. The intensity of the precursor drops down significantly with increasing pyrolysis temperature and is almost completely decomposed at around 400 °C. For the intermediate *t*-BuSSOH, the infrared absorption band is overlapped at lower temperatures by an absorption feature of the precursor and at higher temperatures by the absorption of other pyrolysis products. This influence corrupts the relative intensities depicted in Fig. 3.2 for *t*-BuSSOH. However, the maximum between 400–500°C should be significant, since in the intermediate temperature region the precursor is already decomposed and other pyrolysis products only start to form. The increase of intensity in 2-methylpropene furthermore allows the interpretation as a two-step process. The molecule starts to appear at around 300°C, and its intensity first increases drastically up to about 500°C. At higher pyrolysis temperatures, the intensity further rises up to about 700°C. For even higher temperatures, no additional 2-methylpropene is produced indicating that the thermal decomposition of the precursor (or rather the intermediate *t*-BuSSOH) has reached its maximum. From these results it has to be concluded that 700°C is the optimum pyrolysis temperature to form HSSOH.

The precursor *tert*-butylthiosulfinic acid S-*tert*-butylester was prepared by oxidation of di-*tert*-butyldisulfide in acetic acid with hydrogenperoxide according to the prescription by Netscher and Prinzbach [73]. The synthesis was performed by the workgroup of Prof. Dr. Klein[2], in particular by Y. von Mering.

[1] The data points have been connected by a spline just to facilitate distinguishing the different temperature progressions. Of course, the characteristics of the spline do not reflect the temperature dependence of the pyrolysis products properly.

[2] Department für Chemie, Universität zu Köln, Germany

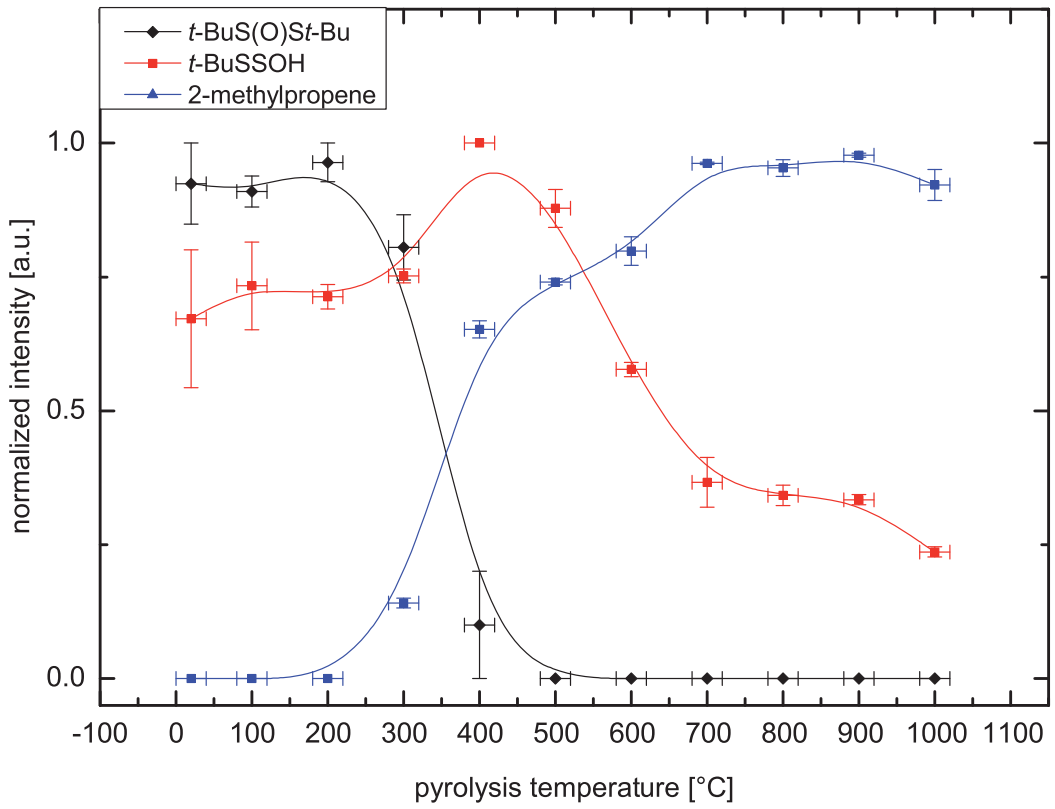

Figure 3.2: Relative intensities of the precursor molecule *t*-BuS(O)S*t*-Bu (black), the intermediate *t*-BuSSOH (red), and the byproduct of both pyrolysis steps 2-methylpropene (blue) as a function of the pyrolysis temperature based on the results of my diploma thesis [58]. The size of the error bars is given by the standard deviation from the mean value of line intensities measured during warm-up and cool-down of the pyrolysis oven.

3.2 Experimental setup for the flash vacuum pyrolysis

The thermal decomposition of *t*-BuS(O)S*t*-Bu leading to the formation of HSSOH in the gas phase, which was described in the previous section, is realized by a pyrolysis oven. The experimental setup for the synthesis of HSSOH during spectroscopic measurements is shown in Fig. 3.3.
The flask containing the liquid precursor is connected to a quarz tube. To increase its vapor pressure, the precursor sample is heated in a water bath to around 40 °C giving rise to a typical pressure of around 15 μbar in the absorption cell. The temperature of the water bath is stabilized by a heating plate which is temperature-controlled by a thermostat. With valve opened, the evaporating precursor molecules get into the quarz tube which is evacuated together with the absorption cell. The thermal decomposition of the precursor molecules in the gas phase takes place in the pyrolysis oven clasping around the quarz tube. The resulting molecules enter the absorption cell and can interact with incoming radiation. As was stated in the last section, the temperature of the pyrolysis oven was chosen to be 700 °C and was controlled via a thermostat.

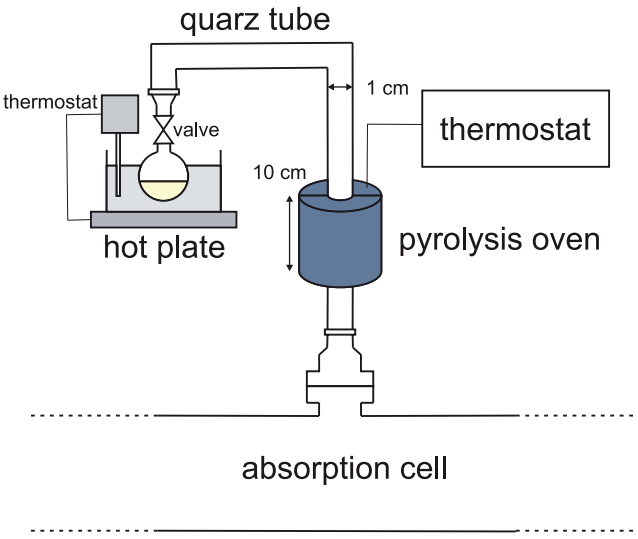

Figure 3.3: Experimental setup for the pyrolysis. The precursor is heated in a water bath to increase its vapor pressure. The thermal decomposition takes place in the pyrolysis oven which is temperature-controlled by a thermostat.

3.3 Stability of HSSOH

As has been stated before, HSSOH is a transient species. To determine its lifetime in the absorption cell, the decay of the HSSOH signal has been monitored as a function of time after simultaneously closing the input valve at the precursor sample and the output valve of the absorption cell. The *cis*-HSSOH $16_{4,13} \leftarrow 16_{3,13}$ rotational transition was chosen for this study since it is one of the most intense transitions in the observed frequency region (see Chapter 5). Fig. 3.4 reveals an exponential decay (red curve) of the peak intensity of the rotational transition (black dots). The fitting result yields a $1/e$ lifetime for HSSOH of approximately 7 s under the conditions of the experiment. Hence, to ensure a stable amount of HSSOH in the absorption cell, spectroscopic measurements have to be performed under flow conditions.

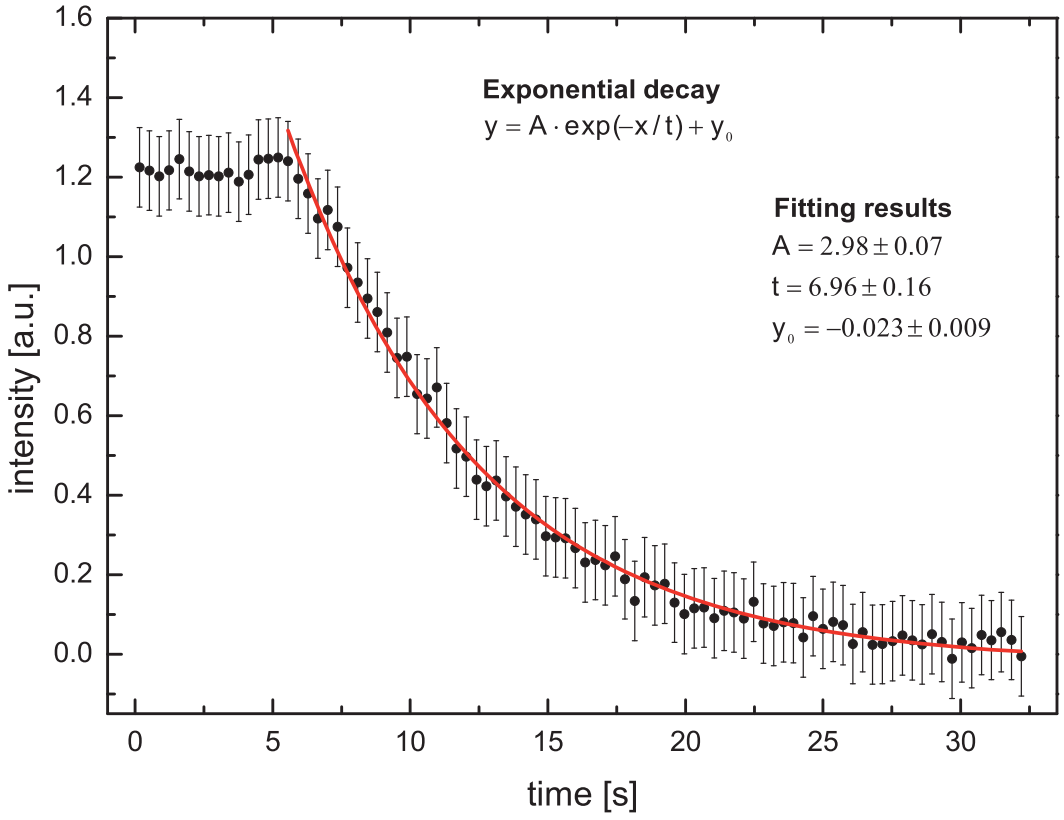

Figure 3.4: Decay of the HSSOH signal. The black dots give the peak intensity of the *cis*-HSSOH $16_{4,13} \leftarrow 16_{3,13}$ rotational transition, whereas the red curve indicates the fit to an exponential decay function.